Geophysical Research Letters

RESEARCH LETTER
10.1029/2021GL094171

Effects of Ocean Optical Properties and Solar Attenuation on the Northwestern Atlantic Ocean Heat Content and Hurricane Intensity

Yangyang Liu[1], **Ruoying He**[2], **and Zhongping Lee**[3]

[1]Xiamen University, Xiamen, China, [2]North Carolina State University, Raleigh, NC, USA, [3]University of Massachusetts, Boston, MA, USA

Key Points:

- The selection of solar attenuation scheme has a significant effect on predictions of ocean heat content and hurricane intensity
- Model experiments using the IOP-based solar attenuation scheme along with satellite observations significantly improve model performance
- Our study highlights the importance of adopting the IOP-based solar attenuation scheme and IOP products in storm forecasting

Supporting Information:

Supporting Information may be found in the online version of this article.

Correspondence to:

R. He,
rhe@ncsu.edu

Citation:

Liu, Y., He, R., & Lee, Z. (2021). Effects of ocean optical properties and solar attenuation on the northwestern Atlantic Ocean heat content and hurricane intensity. *Geophysical Research Letters*, *48*, e2021GL094171. https://doi.org/10.1029/2021GL094171

Received 2 MAY 2021
Accepted 4 JUN 2021

Abstract This study investigated how ocean optical properties and solar attenuation may affect the upper ocean temperature structure and ocean heat content (OHC). We employed a realistic three-dimensional ocean circulation model for the northwestern Atlantic to simulate ocean states during the active Atlantic hurricane season of 2017. Sensitivity experiments were performed by coupling the ocean circulation prediction with either a conventional water type-based solar attenuation model or an inherent optical properties (IOP)-based model. Validations against in-situ ocean temperature observations and remote sensing-derived OHC showed that ocean simulations using the IOP-based model outperformed simulations using the conventional water type-based model in predicting sea surface temperature, upper ocean thermal structure, and OHC. An OHC-hurricane intensity relationship derived for five major hurricanes in 2017 suggests that the ocean optical properties and the application of an appropriate solar attenuation model are important for the forecast of hurricane intensity.

Plain Language Summary In this study, we examined how solar attenuation affects the upper ocean temperature structure and ocean heat content. We employed a realistic three-dimensional ocean circulation model for the northwestern Atlantic to simulate ocean conditions during the active Atlantic hurricane season of 2017. Model experiments were performed by coupling the circulation simulation with either the conventional water type-based solar attenuation model or an inherent optical properties (IOP)-based model. We found that the type of solar attenuation scheme used has a significant effect on the model's ability to predict sea surface temperature, upper thermal structure, ocean heat content, and hurricane intensity. The experiments using the IOP-based model outperformed those using water type-based model. Our study highlights the importance of adopting IOP products from ocean color satellites and the IOP-based solar attenuation model in ocean prediction and storm forecasting.

1. Introduction

The rapid intensification of tropical cyclones is the most challenging aspect of storm forecasting. Sea surface temperature (SST) has not shown to be a dominant factor in intensity forecasting by itself. Rather, the amount of warm, deep water quantified as ocean heat content (OHC) is widely used to describe the amount of energy available to tropical cyclones (Law & Hobgood, 2007; Mainelli et al., 2008; McDougall, 2003; Palmer & Haines, 2009; Schade & Emanuel, 1999; L. K. Shay & Brewster, 2010; Wada & Usui, 2007; Zebiak, 1989). Beginning in 2002, daily OHC analyses have been generated at the National Hurricane Center (NHC). These analyses are used qualitatively for the official NHC intensity forecast, and quantitatively to adjust the Statistical Hurricane Intensity Prediction Scheme forecasts.

OHC, which is defined as the integral of temperature greater than 26°C from the surface to the depth of the 26°C isotherm (Leipper & Volgenau, 1972), can be calculated as:

$$Q = \rho c_p \int_{H_{26}}^{\eta'} \left(T_z - 26^{\circ}\mathrm{C}\right) dz \tag{1}$$

where Q represents OHC ($\mathrm{kJ \cdot cm^{-2}}$), ρ is seawater density, c_p is the specific heat of seawater, η' is sea surface height anomaly, H_{26} is the depth of the 26°C isotherm, and T_z is ocean temperature at depth z. Three-dimensional temperature structures are determined by both ocean advection and surface heat flux. The latter is

dependent upon the attenuation of solar radiation (E_{SR} in $W \cdot m^{-2}$), which is intrinsically related to ocean optical properties.

Various optical models accounting for the attention of E_{SR} with depth have been developed based on either regressions of in-situ bio-optical data (Morel & Antoine, 1994; Paulson & Simpson, 1977) or numerical simulations of the radiative transfer equation (Lee et al., 2005; Ohlmann et al., 2000). The pioneering study by Paulson and Simpson (1977, PS77 hereafter) utilized double exponential functions to describe the propagation of solar radiation from surface to depth, with the coefficients (penetration depths) determined empirically based on Jerlov water types (Jerlov, 1976). The PS77 scheme is widely used as the default attenuation parameterization in community ocean models (e.g., Shchepetkin & McWilliams, 2005). Several recent studies have shown that both water turbidity and solar attenuation can play a significant role in ocean mixed layer dynamics (Kara et al., 2004, 2005a, 2005b), water temperature structures (Cahill et al., 2008), lower atmospheric properties (Jolliff et al., 2012), and hurricane activity in the northwest Pacific (Gnanadesikan et al., 2010). They indicate that improved attenuation parameterization and ocean optical property specification are required.

The advent of global chlorophyll concentration (Chl, in $mg \cdot m^{-3}$) measurement by satellites allowed for the development of Chl-based propagation equations for E_{SR} (Morel & Antoine, 1994; Ohlmann et al., 2000). A basic assumption for the Chl-based scheme is the "Case 1 water" concept (Morel, 1988; Morel & Maritorena, 2001), where the variation of ocean optical properties and the attenuation of E_{SR} with depth can be ascribed by Chl alone. However, the variations of seawater optical properties are not only influenced by phytoplankton (represented by Chl), but also by suspended sediments and colored dissolved organic matter (Sathyendranath et al., 1989). To overcome the limitations of Chl-based regressions, Lee et al. (2005, Lee05 hereafter) developed a propagation model centered on seawater's inherent optical properties (IOPs). Because the attenuation of solar radiation in the upper water column is driven by the total absorption and backscattering coefficients, the IOP-based model generates more accurate vertical distributions of solar radiation in oceanic and coastal waters (Zoffoli et al., 2017). The absorption and backscattering coefficients of the global ocean are now standard products from satellite ocean color remote sensing. This availability allows IOP-based models such as Lee05 to seamlessly quantify the transmission of shortwave solar radiation over a variety of ocean water types, each having different optical properties.

The focus of this study was to examine how ocean optical properties and solar attenuation affect the regional-scale upper ocean temperature structure and ocean heat content. We employed a realistic three-dimensional ocean circulation model for the northwestern Atlantic Ocean to simulate ocean states during the active Atlantic hurricane season of 2017. A suite of three-dimensional sensitivity experiments were performed by coupling the circulation model with either the PS77 water type-based solar attenuation scheme or the Lee05 IOP-based solar attenuation scheme. The resulting OHCs were compared among experiments and also to satellite-derived OHC data product. The relationship between OHC and the intensity of five major hurricanes in 2017 was also examined. Our results show that calculations of Atlantic OHC are very sensitive to ocean optical properties and the solar attenuation schemes used to quantify them in the circulation model. Improvement in tropical storm prediction, therefore, requires accurate upper-ocean optical characterization and advanced ocean models that account for ocean optical properties that are significantly affected by marine biogeochemical processes such as phytoplankton photosynthesis and dynamics of colored dissolved organic matter

2. Method and Data

2.1. Ocean Model

We used the Regional Ocean Modeling System (ROMS; Shchepetkin & McWilliams, 2005) in this study. The model domain (Figure 1) spanned the whole northwestern Atlantic with ~7 km horizontal grid spacing and 36 vertical layers stretched to increase resolution near the surface. The bathymetry was generated using 1 min gridded GEBCO data and smoothed with a linear programming procedure (Sikirić et al., 2009) to remove overly large gradients that may lead to unwanted numerical pressure gradient errors for the model. The model used fourth-order centered advection, with the generic length scale vertical mixing scheme

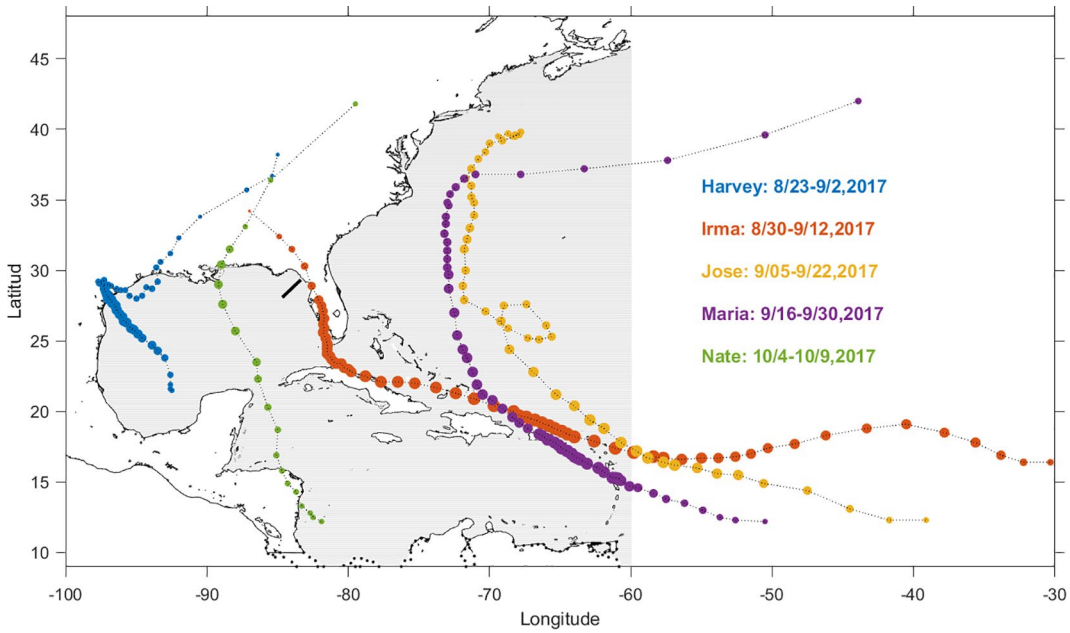

Figure 1. The model domain (shaded) and storm tracks (with symbol sizes scaled by the storm intensity) and the life spans of five major hurricanes in 2017. The thick black line on the west Florida shelf shows the cross-shelf transect where subsurface temperature fields were examined in Figure 2.

(Warner et al., 2005). At its only open boundary on the east, the model was configured to conserve volume with a free-surface Chapman condition, a Flather condition for 2-D momentum, and adaptive nudging and radiation conditions for 3-D momentum and tracers (Marchesiello et al., 2001). Boundary values of ocean states were derived from the daily ocean analysis generated by U.S. Naval Research Laboratory's Global Ocean Forecasting System (GOFS 3.5) implementation of the Hybrid Coordinate Ocean Model (HYCOM) and the Navy Coupled Ocean Data Assimilation (NCODA) system. The European Center for Medium Range Weather Forecast (ECMWF) three-hourly reanalysis was used to generate surface forcing with the bulk flux formulation of Fairall et al. (1996). Interested readers are referred to Zeng and He (2016) for more details of model set up.

2.2. PS77 and Lee05 Schemes of Solar Radiation Attenuation

The PS77 scheme is expressed as:

$$E_{SR}(z) / E_0 = Re^{-z/\xi_1} + (1-R)e^{-z/\xi_2} \quad (2)$$

where $E_{SR}(z)$ is the irradiance at depth z and E_0 is the shortwave radiation at the surface. Based on the Jerlov water type classification (Jerlov, 1976), we examined two extremes of water types: clear open ocean (WTYPE1) and turbid coastal water (WTYPE9). The water clarity parameters (R, ξ_1, ξ_2) in Equation 2 were determined as (0.58, 0.35, 23) for WTYPE1, and as (0.55, 0, 1.51) for WTYPE9. Because these parameters are taken as constants, PS77 does not consider spatial heterogeneity of ocean optical properties in the model domain.

The Lee05 scheme divides the vertical distribution of $E_{SR}(z)$ into two portions: the visible domain of solar radiation (E_{VIS}, 350–700 nm wavelength) and the infrared domain (E_{IR}, 700–2,500 nm wavelength). The vertical distribution of each term in the water column is described by exponential functions, and $E_{SR}(z)$ in the Lee05 scheme is:

$$E_{SR}(z) = F_{VIS}e^{-K_{VIS}(IOP,z,\theta_a)z} + (1-F_{VIS})e^{-K_{IR}(z,\theta_a)z} \quad (3)$$

where F_{VIS} is the ratio of $E_{VIS}(0^-)/E_0$ with a general value of 0.47. $K_{VIS}(z)$ and $K_{IR}(z)$ are the diffuse attenuation coefficients varying with depth and sun angle θ_a for $E_{VIS}(z)$ and $E_{IR}(z)$, respectively. Because IOPs control the attenuation of solar radiation in the water column, $K_{VIS}(z)$ in Lee05 is modeled as a function of depth and the ocean's absorption and backscattering coefficients:

$$K_{VIS}\left(z, IOP, \theta_a\right) = K_1\left(IOP\right) + \frac{K_2\left(IOP\right)}{\sqrt{1+z}} \tag{4}$$

where K_1 and K_2 are functions of ocean's absorption $a(490)$ and backscattering $b_b(490)$ coefficients at 490 nm:

$$K_1\left(IOP, \theta_a\right) = \left[\chi_0 + \chi_1\left(a\left(490\right)\right)^{0.5} + \chi_2 b_b\left(490\right)\right]\left(1 + \alpha_0 \sin\left(\theta_a\right)\right) \tag{5}$$

$$K_2\left(IOP, \theta_a\right) = \left[\zeta_0 + \zeta_1\left(a\left(490\right)\right) + \zeta_2 b_b\left(490\right)\right]\left(\alpha_1 + \alpha_2 \cos\left(\theta_a\right)\right)$$

$\chi 0$, $\chi 1$, $\chi 2$, $\zeta 0$, $\zeta 1$, $\zeta 2$, $\alpha 0$, $\alpha 1$, and $\alpha 2$ are model constants tuned by fitting numerical simulations using HydroLight (Mobley, 1995), and can be found in Lee et al. (2005). Because no $a(490)$ and $b_b(490)$ field observation were available for the entire northwestern Atlantic domain, we used NASA 9 km resolution $a(488)$ and $b_b(488)$ products derived from MODIS using Lee et al. (2005) scheme as inputs for the calculation of KVIS. These monthly satellite observations are linearly interpolated to each ocean model integration time step, providing seamless quantification of the optical properties in complex ocean water masses from estuaries to the open ocean. For the attenuation coefficient in the IR domain (700–2,500 nm), KIR is modeled as

$$K_{IR}\left(z, \theta_a\right) = \left(0.560 + \frac{2.304}{\left(0.001 + z\right)^{0.65}}\right)\left(1 + 0.002\theta_a\right) \tag{6}$$

Because 99% of infrared solar radiation is absorbed within the top 1.23 m (Morel & Antoine, 1994), K_{IR} is considered not varying with ocean constituents.

In the supporting information, we provide a comparison of one-dimensional irradiance transmission profiles generated by the three scenarios using PS77 (WTYPE1 and WTYPE9) and Lee05. WTYPE1 (WTYPE9) represents clear, open-ocean (turbid, coastal ocean). They are two end-members water masses presented in our NW Atlantic study domain. As expected, the PS77 WTYPE9 case had the strongest attenuation and shortwave transmission was reduced to near zero within the top 10 m. In contrast, light attenuation in the PS77 WTYPE1 case was the weakest, with shortwave transmission not reaching near zero until about 100 m below the surface. The light transmission produced by the Lee05 scheme fell between them.

Liu et al. (2020) explored the impact of transmission schemes on upper ocean temperature and mixing using a 1-D ocean model. Our study expands the investigation in a 3-D ocean over the entire Northwestern Atlantic and focuses on OHC. Our control modeling experiment applied the Lee05 scheme for irradiance attenuation in the water column, while the two sensitivity experiments used the PS77 scheme (WTYPE1 and WTYPE9). In all three experiments, the three-dimensional model simulations were initialized with daily global HYCOM NCODA ocean reanalysis and ran from January 1 to December 31, 2017. Detailed ROMS model validation and analyses on model temperature fields are given in the supporting information. Herein, we focus on the modeled OHC analysis during the 2017 hurricane season (June 1 to November 30).

2.3. NOAA Satellite-Derived OHC

NOAA routinely produces 1/4° daily OHC analysis for the North Atlantic. This operational analysis uses sea surface height anomaly (SSHA) from satellite altimeters, sea surface temperatures (SST) from the GEO-POLAR Blended product (Maturi et al., 2017), a regional temperature and salinity climatology for the Atlantic, and a 2.5-layer model to project surface satellite observations to subsurface thermal structures. Daily depth of the 26°C isotherm (D26) and OHC are subsequently derived for the resultant three-dimensional ocean temperature fields routinely generated at NOAA. Interested readers are referred to L. L. Shay et al. (2019) for

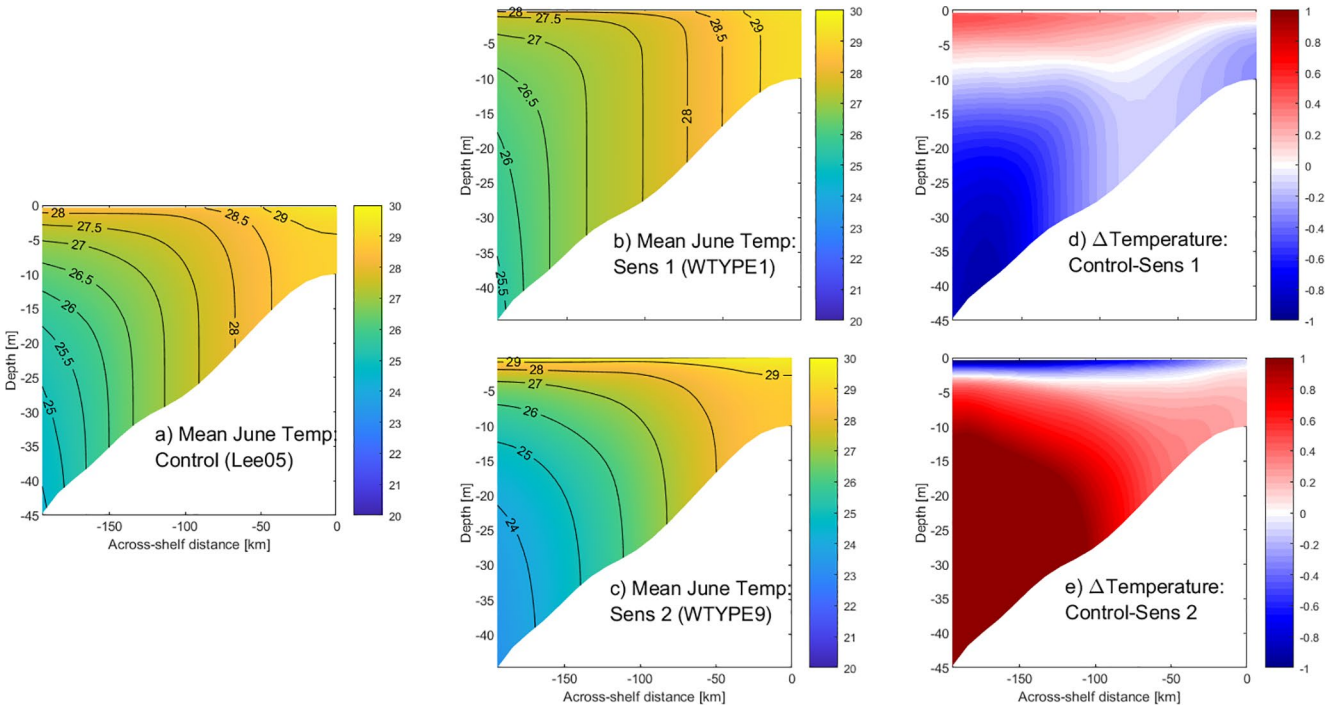

Figure 2. Cross-shelf transects showing the June 2017 mean temperature fields (°C, shown in color shading and contour lines) modeled by simulations using (a) Lee05, (b) PS77 WTYPE1, and (c) PS77 WTYPE9. Also shown are the June mean temperature differences between (d) simulations using Lee05 and WTYPE1, and (e) simulations using Lee05 and WTYPE9.

technical details of this product. In this study, we used this satellite-derived OHC from June 1 to November 30, 2017 as an independent dataset to evaluate OHCs generated by our ROMS model simulations.

3. Results

3.1. Subsurface Temperature

The impact of different irradiance transmission schemes on the subsurface temperature fields were examined along a cross-shelf transect on the west Florida shelf (see location in Figure 1). Simulated June subsurface temperature fields from all three experiments (Control: Lee05; Sensitivity 1: PS77 WTYPE1; Sensitivity 2: PS 77 WTYPE9) shared several common features (Figure 2). First, the water was thermally stratified in June. The monthly mean temperature field had ~4–5°C difference between the surface and water at 45 m. Second, the depth-averaged temperature is higher in the shallow water near the coast than in the deep water further offshore. This is because in a depth-average sense, the monthly mean ocean temperature variation could be represented by $\partial T / \partial t = Q(t) / \left[\rho \cdot Cp \cdot H\right]$, where $Q(t)$ is the net surface flux, ρ is water density, Cp is ocean water heat capacity, and H is water depth. Thus vertically integrated water column temperature variations are inversely proportional to the water depth (He & Weisberg, 2003).

Nevertheless, model sensitivity to different irradiance transmission schemes was highlighted by the detailed subsurface temperature structure differences between the simulation pairs. Because of the higher attenuation in Lee05 (Figure 2a), solar radiation could not penetrate as deep as it could in PS77 WTYPE1 (Figure 2b). The shortwave radiation was thus distributed more in the upper water column, leading to a warmer layer in the upper 10 m, and a colder layer between 10 and 45 m in Lee05 case (Figure 2d). A nearly opposite pattern was seen in the difference between Lee05 and PS77 WTYPE9 (Figure 2c), where Lee05 created a colder (warmer) upper (lower) water column than PS77 WTYPE9 (Figure 2e). This was because shortwave radiation was trapped in the upper layer by the higher attenuation in PS77 WTYPE9, which creates a warmer surface layer and a colder deep layer in the Sensitivity 2 experiment relative to the Control.

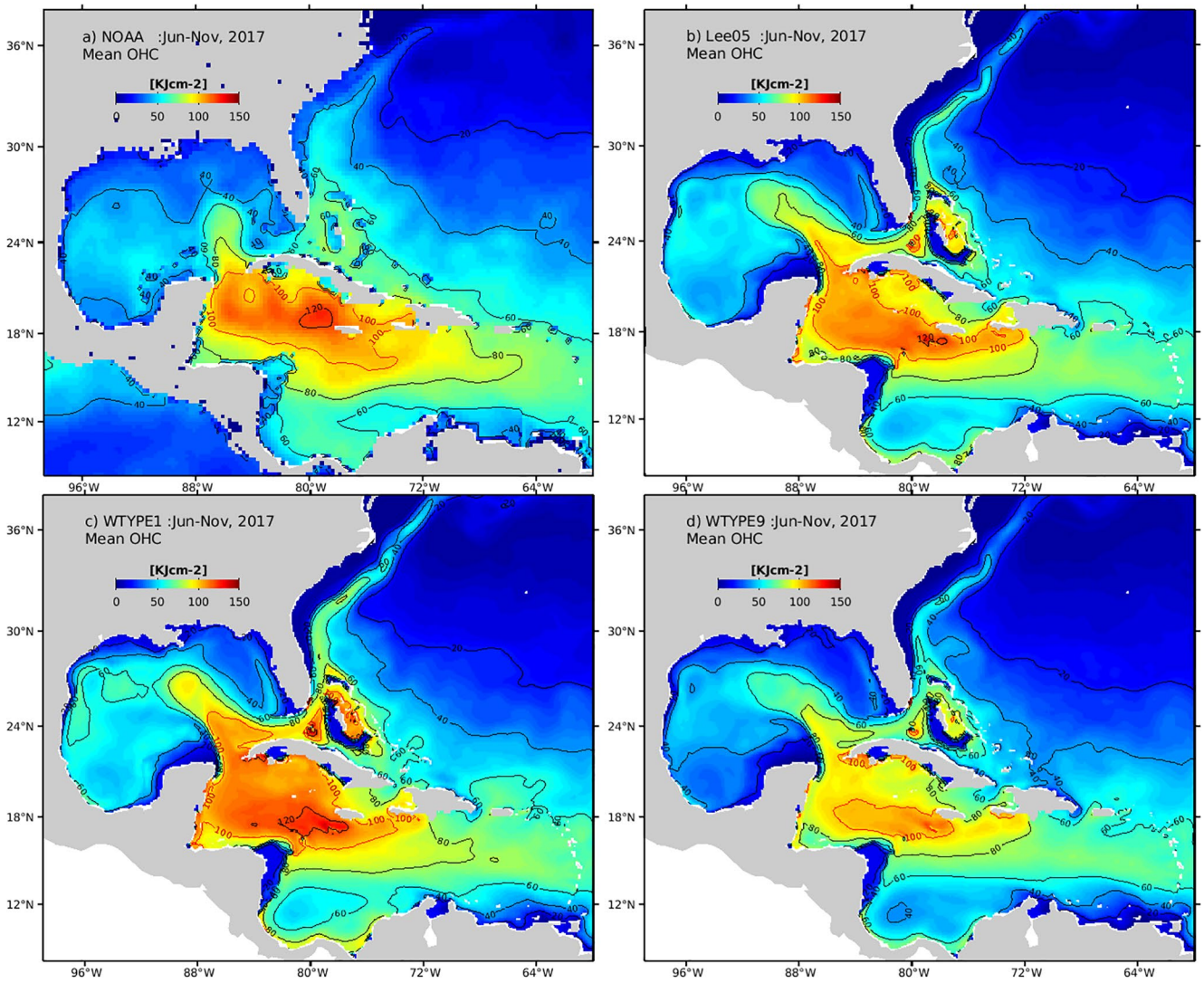

Figure 3. Comparison of the hurricane season (June 1 to November 30) mean OHC $\left(\mathrm{kJ}\cdot\mathrm{cm}^{-2}\right)$ obtained from (a) NOAA product, (b) Control (Lee05) model run, (c) Sensitivity 1 (PS77, WTYPE1) model run, and (d) Sensitivity 2 (PS77, WTYPE9) model run. The 100 $\mathrm{kJ}\cdot\mathrm{cm}^{-2}$ contor (red line) is used to define the area with the maximum OHC throughout the hurricane season.

In both comparisons, the absolute temperature differences between Lee05 Control and PS77 sensitivity experiments were significant, with values up to 1°C.

3.2. OHC

The difference in modeled subsurface temperature fields was magnified further when we calculated daily OHC using Equation 1. This is because the solar radiation can penetrate deeper and thus affect a larger portion of water column in WTYPE 1 case than in Lee05 case and WTYPE 9 case. OHC, being an integral quantity of the upper ocean thermal field, is thus a more appropriate and revealing variable than SST in quantifying ocean heat distribution. For both the Lee05 Control and Sensitivity experiments, the resultant daily OHC fields were averaged over the six months between June 1 and November 30 to generate the "hurricane season" mean OHC and compared with their observational counterpart obtained from the daily NOAA satellite-derived OHC product (Figure 3a).

Several limitations in both satellite product and model simulation results can be seen in these mean OHC fields. First, because the satellite product has a coarse 0.25° resolution, it cannot resolve coastal ocean OHC

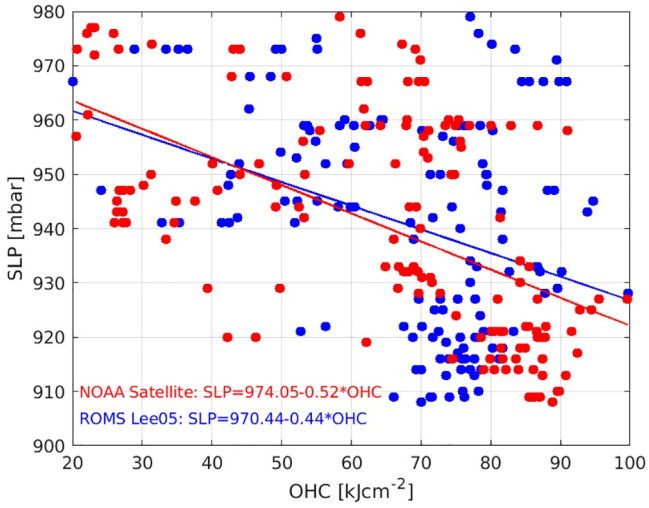

Figure 4. The relationship between observed hurricane sea level pressure (SLP) and satellite-derived (red) and the Control model-simulated (blue) OHC sampled for all five major hurricanes in August through October 2017. The 95% confidence intervals for the linear regression coefficients used in the satellite-based (the Control model simulation based) OHC-SLP models are (965.81 982.29) ([956.27 984.61]) for the intercept and (–0.64 –0.39) ([–0.64 –0.24]) for the slope. Their corresponding p-value and r-squared value are 3.06×10^{-14} and 0.32 (3.28×10^{-5} and 0.12), respectively.

well. The OHC in several shelf regions (e.g., the South Atlantic Bight, the West Florida shelf, and the Campeche Bank) were significantly larger than their model counterparts. Second, all ROMS simulations were non-data assimilative, so the timing of the Loop Current eddy separation was not constrained by observations (e.g., SSHA from satellite altimeters). As a result, the simulated Loop Current penetrated farther into the Gulf of Mexico than what the satellite product showed, increasing the simulated OHC and the area with large OHC in the Gulf of Mexico. Nevertheless, all the OHCs resembled each other in capturing the Atlantic Warm Pool (AWP). The AWP is a large body of warm water that extends into the Gulf of Mexico, Caribbean Sea, and western tropical North Atlantic. In addition to providing ocean heat energy to existing tropical cyclones/hurricanes, the AWP was associated in earlier studies with a decrease in sea level pressure and an increase in atmospheric convection and cloudiness. This leads to weak tropospheric vertical wind shear, thus promoting new Atlantic tropical cyclone/hurricane activity (Enfield & Cid-Serrano, 2010; Wang et al., 2006, 2008).

The Control run using Lee05 produced the seasonal mean OHC distribution in terms of the AWP magnitude, spatial pattern, and size that most closely matched the independent, satellite-derived OHC. The linear regression coefficient and the root-mean-squared difference (RMSD) between the two OHC fields were 0.97 and 15.6 kJ · cm^{-2}, respectively. The Sensitivity run using PS77 WTYPE1 generated a warmer, larger AWP that extended further into the Caribbean coastal regions and the Gulf of Mexico. Its linear regression coefficient and the root-mean-squared magnitude difference relative to the satellite-derived OHC were 1.05 and 16.9 kJ · cm^{-2}, respectively. In contrast, the Sensitivity run using PS77 WTYPE9 generated a cooler, smaller AWP that shrank to the central Caribbean Sea. The linear regression coefficient and the root-mean-squared magnitude difference relative to the satellite-derived OHC were 0.87 and 17.2 kJ · cm^{-2}, respectively. These regression and RMSD results suggest that the choice of the irradiance transmission scheme can introduce notable significant uncertainty in prediction of OHC and characteristics of the AWP, and Lee05 is superior to PS77 in accounting for the impact of ocean optical properties and solar attenuation in the northwestern Atlantic.

3.3. OHCs Associated With Major Hurricanes

Next, we sampled the specific satellite-derived and model-simulated OHCs at the same times and locations where five major hurricanes (Figure 1) moved across the northwestern Atlantic between August 23 and October 9, 2017. Because lower sea level pressure (SLP) means stronger hurricane intensity, we calculated regressions between the observed hurricane SLPs and two OHCs, one from a NOAA satellite product and the other from the Control (Lee05) model simulation (Figure 4). In both cases and to the first order, a similar linear inverse relationship was found, confirming that the hurricane intensity of the five hurricanes studied was generally proportional to the underlying OHC, as expected.

Point-by-point comparison of OHCs along the five hurricane tracks showed the NOAA satellite-derived and the Control (Lee05) model-simulated OHC shared similar magnitude and spatial variations (Figure 5). However, compared with the Control run, the OHCs produced by the Sensitivity model runs were over-predicted (under-predicted) by up to 30% when PS77 WTYPE1 (WTYPE9) was used. Based on the above-mentioned OHC-SLP semi-linear relationship, a 30% OHC change is proportional to about 20 mb SLP change, which is greater than the difference in SLP between consecutive Saffir-Simpson hurricane Categories (https://www.ssd.noaa.gov/PS/TROP/CI-chart.html). Thus choice of the irradiance transmission scheme can cause a significant discrepancy not only in simulated OHC, but also in predicted intensity/category of tropical cyclones.

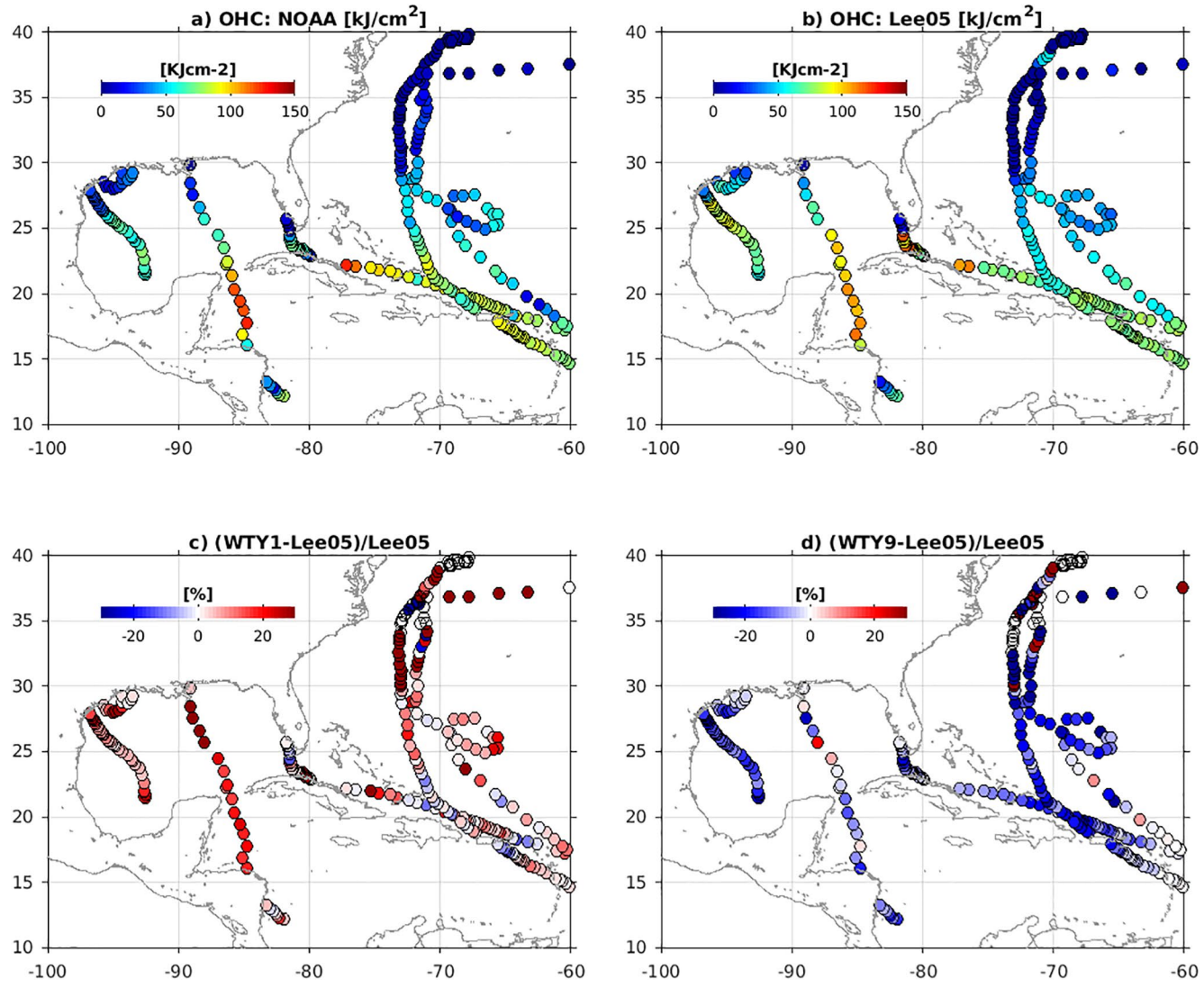

Figure 5. Comparisons of (a) NOAA satellite-derived OHC (kJ · cm^{-2}) and (b) Control (Lee05) model-simulated OHC sampled at the same times and locations where five major hurricanes translated through the northwestern Atlantic in August through October 2017. Also shown are the percent difference between OHCs simulated by (c) Sensitivity 1 (WTYPE1) and the Control and (d) Sensitivity 2 (WTYPE9) and the Control.

4. Summary and Conclusion

In this study, we examined how ocean optical properties and solar attenuation affect the upper ocean temperature structure and ocean heat content. We employed a realistic three-dimensional ocean circulation model for the northwestern Atlantic to simulate ocean states during the active Atlantic hurricane season of 2017. A suite of sensitivity experiments were performed by coupling the circulation model with either the PS77 water-type solar attenuation scheme or the Lee05 IOP-based solar attenuation scheme.

PS77 is a conventional solar attenuation scheme adopted by many community ocean circulation models and air-sea coupled models. It accounts for the water column transmittance of solar radiation with simple exponential functions based on a single water optical type, where the irradiance attenuation coefficients for broad shortwave solar radiation are treated as constants over the entire model domain. Such a simplification does not match the transmission of solar radiation in the heterogeneous oceanic environment in reality, where spatially varying optical properties are present and interleaving. Unlike PS77, Lee05 is an IOP-based optical model with solar radiation divided into in visible (wavelength <700 nm) and infrared (wavelength >700 nm) bands, where the spatial variations of ocean optical properties and the vertical variation

of the attenuation coefficients are fully considered. The model requires observed absorption and backscattering coefficients, which are adequately available now from routine satellite ocean color measurements.

Results from our model experiments were validated against both in-situ temperature observations (see the supporting information) and remote sensing-derived OHC analysis. We found that the selection of solar attenuation scheme had a significant effect on a model's accuracy in predicting SST, upper thermal structure, AWP, and OHC. The Control simulation using the Lee05 scheme outperformed the two Sensitivity runs using the PS77 scheme. For OHC in particular, up to a 30% difference was calculated when using the PS77 scheme as opposed to the Lee05 scheme in the ocean circulation simulation. A 30% OHC change is proportional to about 20 mb SLP change, based on the OHC-hurricane intensity linear relationship we derived for the five major hurricanes in 2017, which is greater than the difference in SLP between consecutive Saffir-Simpson hurricane Categories. Therefore, ocean optical properties and application of realistic attenuation schemes in ocean models can play a significant role in hurricane intensity forecasts.

Our study highlights the importance of adopting the IOP-based solar attenuation model in ocean prediction and storm forecasting. The connections identified in this study among ocean optics, ocean thermal fields, and OHC deserve more detailed investigation, as OHC plays a major role in modulating not only summer tropical storms (e.g., Mainelli et al., 2008), but also winter extratropical storms (e.g., Nelson & He, 2012,). Ocean optics are also affected by marine biogeochemical processes such as phytoplankton photosynthesis and dynamics of colored dissolved organic matter. How the intrinsic relationship between optics and ocean circulation evolves in a warming climate to influence ocean heat budgets and storms is an intriguing topic. Understanding it clearly requires more coupled modeling experiments in conjunction with a coordinated, high-frequency observing network that can simultaneously collect water column observations of ocean physical, optical, and biogeochemical properties.

Data Availability Statement

Model simulation output used in this study is available upon request. HYCOM NCODA reanalysis data are available at https://www.hycom.org/dataserver/gofs-3pt0/analysis. NASA 9-km resolution MODIS $a(488)$ and $b_b(488)$ products are available at http://oceandata.sci.gsfc.nasa.gov/MODIS-Aqua/Mapped/Monthly_Climatology/9km. NOAA satellite-derived OHC data are available at https://www.ospo.noaa.gov/Products/ocean/ohc_natl.html. Buoy-observed sea surface temperature data are available at https://www.ndbc.noaa.gov/. Hurricane track and intensity data are available at http://fermi.jhuapl.edu/hurr/17/17.html.

Acknowledgments
YL acknowledges funding support from the National Natural Science Foundation of China (#41890803, #41830102) and China Scholarship Council. RH acknowledges funding support from NSF grant OCE-1559178271 and OCE-1851421, NOAA grant NA16NOS0120028, North Carolina Renewable Ocean Energy program, and the support by the USGS/Marine Hazards and Resources Program, and by Congressional appropriations through the Additional Supplemental Appropriations for Disaster Relief Act of 2019 (H.R. 2157). Jennifer Warrillow is acknowledged for her editorial assistance.

References

Cahill, B., Schofield, O., Chant, R., Wilkin, J., Hunter, E., Glenn, S., & Bissett, P. (2008). Dynamics of turbid buoyant plumes and the feedbacks on near-shore biogeochemistry and physics. *Geophysical Research Letters*, *35*, L10605. https://doi.org/10.1029/2008GL033595

Enfield, D. B., & Cid-Serrano, L. (2010). Secular and multidecadal warmings in the North Atlantic and their relationships with major hurricane activity. *International Journal of Climatology: A Journal of the Royal Meteorological Society*, *30*(2), 174–184.

Fairall, C. W., Bradley, E. F., Rogers, D. P., Edson, J. B., & Young, G. S. (1996). Bulk parameterization of air-sea fluxes for tropical ocean-global atmosphere coupled-ocean atmosphere response experiment. *Journal of Geophysical Research: Oceans*, *101*(C2), 3747–3764. https://doi.org/10.1029/95jc03205

Gnanadesikan, A., Emanuel, K., Vecchi, G. A., Anderson, W. G., & Hallberg, R. (2010). How ocean color can steer Pacific tropical cyclones. *Geophysical Research Letters*, *37*, L18802. https://doi.org/10.1029/2010GL044514

He, R., & Weisberg, R. H. (2003). West Florida Shelf circulation and temperature budget for the 1998 fall transition. *Continental Shelf Research*, *23*(8), 777–800. https://doi.org/10.1016/S0278-4343(03)00028-1

Jerlov, N. G. (1976). *Marine optics*. Elsevier.

Jolliff, J. K., Smith, T. A., Barron, C. N., deRada, S., Anderson, S. C., Gould, R. W., & Arnone, R. A. (2012). The impact of coastal phytoplankton blooms on ocean-atmosphere thermal energy exchange: Evidence from a two-way coupled numerical modeling system. *Geophysical Research Letters*, *39*, L24607. https://doi.org/10.1029/2012GL053634

Kara, A. B., Hurlburt, H. E., Rochford, P. A., & O'Brien, J. J. (2004). The impact of water turbidity on the interannual sea surface temperature simulations in a layered global ocean model. *Journal of Physical Oceanography*, *34*, 345–359. https://doi.org/10.1175/1520-0485(2004)034<0345:tiowto>2.0.co;2

Kara, A. B., Wallcraft, A. J., & Hurlburt, H. E. (2005a). A new solar radiation penetration scheme for use in ocean mixed layer studies: An application to the Black Sea using a fine-resolution Hybrid Coordinate Ocean Model (HYCOM). *Journal of Physical Oceanography*, *35*, 13–32. https://doi.org/10.1175/jpo2677.1

Kara, A. B., Wallcraft, A. J., & Hurlburt, H. E. (2005b). How does solar attenuation depth affect the ocean mixed layer? Water turbidity and atmospheric forcing impacts on the simulation of seasonal mixed layer variability in the turbid Black Sea. *Journal of Climate*, *18*, 389–409. https://doi.org/10.1175/jcli-3159.1

Law, K. T., & Hobgood, J. S. (2007). A statistical model to forecast short-term Atlantic hurricane intensity. *Weather and Forecasting*, *22*(5), 967–980. https://doi.org/10.1175/waf1027.1

Lee, Z., Du, K., Arnone, R., Liew, S., & Penta, B. (2005). Penetration of solar radiation in the upper ocean: A numerical model for oceanic and coastal waters. *Journal of Geophysical Research: Oceans*, *110*(C9). https://doi.org/10.1029/2004jc002780

Leipper, D. F., & Volgenau, D. (1972). Hurricane heat potential of the Gulf of Mexico. *Journal of Physical Oceanography*, *2*(3), 218–224. https://doi.org/10.1175/1520-0485(1972)002<0218:hhpotg>2.0.co;2

Liu, T., Lee, Z., Shang, S., Xiu, P., Chai, F., & Jiang, M. (2020). Impact of transmission scheme of visible solar radiation on temperature and mixing in the upper water column with inputs for transmission derived from ocean color remote sensing. *Journal of Geophysical Research: Oceans*, *125*(7). https://doi.org/10.1029/2020jc016080

Mainelli, M., DeMaria, M., Shay, L. K., & Goni, G. (2008). Application of oceanic heat content estimation to operational forecasting of recent Atlantic category 5 hurricanes. *Weather and Forecasting*, *23*(1), 3–16. https://doi.org/10.1175/2007waf2006111.1

Marchesiello, P., McWilliams, J. C., & Shchepetkin, A. (2001). Open boundary conditions for long-term integration of regional oceanic models. *Ocean Modelling*, *3*(1–2), 1–20. https://doi.org/10.1016/s1463-5003(00)00013-5

Maturi, E., Harris, A., Mittaz, J., Sapper, J., Wick, G., Zhu, X., et al. (2017). A new high-resolution sea surface temperature blended analysis. *Bulletin of the American Meteorological Society*, *98*(5), 1015–1026. https://doi.org/10.1175/bams-d-15-00002.1

McDougall, T. J. (2003). Potential enthalpy: A conservative oceanic variable for evaluating heat content and heat fluxes. *Journal of Physical Oceanography*, *33*(5), 945–963. https://doi.org/10.1175/1520-0485(2003)033<0945:peacov>2.0.co;2

Mobley, C. (1995). *Hydrolight 3.0 user's guide* (Final Report).

Morel, A. (1988). Optical modeling of the upper ocean in relation to its biogenous matter content (case I waters). *Journal of Geophysical Research*, *93*(C9). https://doi.org/10.1029/jc093ic09p10749

Morel, A., & Antoine, D. (1994). Heating rate within the upper ocean in relation to its bio-optical state. *Journal of Physical Oceanography*, *24*(7), 1652–1665. https://doi.org/10.1175/1520-0485(1994)024<1652:hrwtuo>2.0.co;2

Morel, A., & Maritorena, S. (2001). Bio-optical properties of oceanic waters: A reappraisal. *Journal of Geophysical Research: Oceans*, *106*(C4), 7163–7180. https://doi.org/10.1029/2000jc000319

Nelson, J., & He, R. (2012). Effect of the Gulf Stream on winter extratropical cyclone outbreaks. *Atmospheric Science Letters*, *13*(4), 311–316. https://doi.org/10.1002/asl.400

Ohlmann, J. C., Siegel, D. A., & Mobley, C. D. (2000). Ocean radiant heating. Part I: Optical influences. *Journal of Physical Oceanography*, *30*(8), 1833–1848. https://doi.org/10.1175/1520-0485(2000)030<1833:orhpio>2.0.co;2

Palmer, M. D., & Haines, K. (2009). Estimating oceanic heat content change using isotherms. *Journal of Climate*, *22*(19), 4953–4969. https://doi.org/10.1175/2009jcli2823.1

Paulson, C. A., & Simpson, J. J. (1977). Irradiance measurements in the upper ocean. *Journal of Physical Oceanography*, *7*(6), 952–956. https://doi.org/10.1175/1520-0485(1977)007<0952:imituo>2.0.co;2

Sathyendranath, S., Prieur, L., & Morel, A. (1989). A three-component model of ocean color and its application to remote sensing of phytoplankton pigments in coastal waters. *International Journal of Remote Sensing*, *10*(8), 1373–1394. https://doi.org/10.1080/01431168908903974

Schade, L. R., & Emanuel, K. A. (1999). The ocean's effect on the intensity of tropical cyclones: Results from a simple coupled atmosphere–ocean model. *Journal of the Atmospheric Sciences*, *56*(4), 642–651. https://doi.org/10.1175/1520-0469(1999)056<0642:toseot>2.0.co;2

Shay, L. K., & Brewster, J. K. (2010). Oceanic heat content variability in the eastern Pacific Ocean for hurricane intensity forecasting. *Monthly Weather Review*, *138*(6), 2110–2131. https://doi.org/10.1175/2010mwr3189.1

Shay, L. L., Brewster, J., Maturi, E., Donahue, D., Meyers, P., & McCaskill, C. (2019). *ATBD: Satellite-derived ocean heat content. Satellite products and service review board report*. https://www.ospo.noaa.gov/Products/ocean/assets/ATBD_OHC_NESDIS_V3.2.pdf

Shchepetkin, A. F., & McWilliams, J. C. (2005). The regional oceanic modeling system (ROMS): A split-explicit, free-surface, topography-following-coordinate oceanic model. *Ocean Modelling*, *9*(4), 347–404. https://doi.org/10.1016/j.ocemod.2004.08.002

Sikirić, M. D., Janeković, I., & Kuzmić, M. (2009). A new approach to bathymetry smoothing in sigma-coordinate ocean models. *Ocean Modelling*, *29*(2), 128–136.

Wada, A., & Usui, N. (2007). Importance of tropical cyclone heat potential for tropical cyclone intensity and intensification in the western North Pacific. *Journal of Oceanography*, *63*(3), 427–447. https://doi.org/10.1007/s10872-007-0039-0

Wang, C., Enfield, D. B., Lee, S.-k., & Landsea, C. W. (2006). Influences of the Atlantic warm pool on Western Hemisphere summer rainfall and Atlantic hurricanes. *Journal of Climate*, *19*(12), 3011–3028. https://doi.org/10.1175/jcli3770.1

Wang, C., Lee, S. K., & Enfield, D. B. (2008). Atlantic warm pool acting as a link between Atlantic multidecadal oscillation and Atlantic tropical cyclone activity. *Geochemistry, Geophysics, Geosystems*, *9*(5). https://doi.org/10.1029/2007gc001809

Warner, J. C., Sherwood, C. R., Arango, H. G., & Signell, R. P. (2005). Performance of four turbulence closure models implemented using a generic length scale method. *Ocean Modelling*, *8*(1–2), 81–113. https://doi.org/10.1016/j.ocemod.2003.12.003

Zebiak, S. E. (1989). Oceanic heat content variability and El Niño cycles. *Journal of Physical Oceanography*, *19*(4), 475–486. https://doi.org/10.1175/1520-0485(1989)019<0475:ohcvae>2.0.co;2

Zeng, X., & He, R. (2016). Gulf Stream variability and a triggering mechanism of its large meander in the South Atlantic Bight. *Journal of Geophysical Research: Oceans*, *121*(11), 8021–8038. https://doi.org/10.1002/2016jc012077

Zoffoli, M. L., Lee, Z., Ondrusek, M., Lin, J., Kovach, C., Wei, J., & Lewis, M. (2017). Estimation of transmittance of solar radiation in the visible domain based on remote sensing: Evaluation of models using in situ data. *Journal of Geophysical Research: Oceans*, *122*(11), 9176–9188. https://doi.org/10.1002/2017jc013209